Reaction Synthesis/Dynamic Compaction of Titanium Diboride

D.A. HOKE, M.A. MEYERS, L.W. MEYER, and G.T. GRAY III

A new method for producing dense compacts of titanium diboride is described. This approach combines reaction synthesis with a high velocity forging step (5 to 15 m/s impact velocity) to achieve densification and near-net shape. By combining synthesis and densification, titanium diboride disks with over 96 pct of the theoretical density were produced. The highly exothermic (279.6 to 324.0 kJ/mol) synthesis reaction between titanium and boron produces temperatures of approximately 3000 K, at which the material is ductile and forgeable in a high-speed machine. The mechanical properties (quasi-static and dynamic) of reaction-synthesized/dynamically compacted titanium diboride are determined and compared with that of conventionally hot-pressed material.

I. INTRODUCTION

PRODUCTION of high-temperature refractory materials by conventional powder-consolidation methods involves energy- and time-intensive techniques. Typically, hot pressing requires long exposures to high temperatures, with low production rates. Recently, a novel materials processing technique termed self-propagating high-temperature synthesis (SHS), combustion synthesis, or reaction synthesis has been used to produce a wide variety of refractory materials, including ceramics, ceramic composites, and intermetallic compounds.[1–4] The process involves the direct or indirect synthesis of a material *via* a high-temperature thermochemical reaction. The high temperatures encountered during the synthesis reactions often result in the expulsion of any volatile impurities or moisture that may be found in the starting powders. Since the starting powders have an initial porosity, the synthesized compound has a higher density than the weighted average of the reactants, but due to the expulsion of impurity gases, escape channels are produced and a porous product is formed. Therefore, reaction-synthesized materials without an external densification step can exhibit up to 50 pct porosity.

Since high-temperature synthesis often results in the product material being raised to a temperature well above its ductile-brittle transition temperature (DBTT), the porosity can be reduced, or eliminated, if the SHS product is consolidated while it remains at a temperature above its DBTT. Using explosively driven flyer plates as a technique to consolidate the porous SHS product, Niiler *et al.*[5] successfully produced TiC and TiB_2 ceramics in excess of 98 pct of theoretical density. Holt and Munir[6] successfully densified TiC to 97 pct of theoretical density by uniaxial hot pressing following the SHS reaction. Recently, LaSalvia *et al.*[7] showed that TiC could be densified in excess of 96 pct of the theoretical density by dynamically compacting the SHS product using a high-velocity forging machine. The principal advantages of the high-velocity forging machine are that it is relatively safe, affords near-net shape capability, and lends itself to high-rate production runs with little or no down time between parts.

The principal objective of this research was to demonstrate that the dynamic compaction process developed for reaction-synthesized TiC[7] can be applied to TiB_2. Process variables such as specimen containment and composition were found to be critical aspects in the successful densification of the ceramic.

II. EXPERIMENTAL PROCEDURE

High-purity (99.7 pct) titanium (Micron Metals, Inc., Salt Lake City, UT), 99.3 pct crystalline boron (Hermann C. Starck, Berlin), and 99.5 pct titanium diboride (Johnson Matthey, Seabrook, NH) powders were dry mixed in a ball mill for 4 hours. The three starting powder sizes were −325 mesh, corresponding to a particle size smaller than 44 μm. In order to ensure that the final product composition fell in the region of the binary phase diagram where TiB_2 occurs, the titanium/boron powders were mixed in 33/67 at. pct ratios. Presynthesized titanium diboride was added (22.5 wt pct) as a diluent to the system in order to obtain a well-controlled reaction suitable for the experimental setup and to insure the integrity of the compact after reaction. The mixed powders were uniaxially pressed into green compacts having a diameter of 63.5 mm and an approximate height of 38 mm, corresponding to a green density of approximately 65 to 70 pct of theoretical.

The powder compact was placed into a reaction-consolidation fixture which provided both high-temperature insulation and containment of the sample during the synthesis and subsequent compaction step (Figure 1). The fixture consisted of a mild steel outer

D.A. HOKE, Graduate Student, and M.A. MEYERS, Professor of Materials Science, are with the University of California–San Diego, La Jolla, CA 92093-0411. L.W. MEYER, Research Leader, is with the Fraunhofer-Institut fur Angewandte Materialforschung (IFAM), D-2820 Bremen 77, Federal Republic of Germany. G.T. GRAY III, Technical Staff Member, is with Los Alamos National Laboratory, Los Alamos, NM 87545.

This paper is based on a presentation made in the symposium "Reaction Synthesis of Materials" presented during the TMS Annual Meeting, New Orleans, LA, February 17–21, 1991, under the auspices of the TMS Powder Metallurgy Committee.

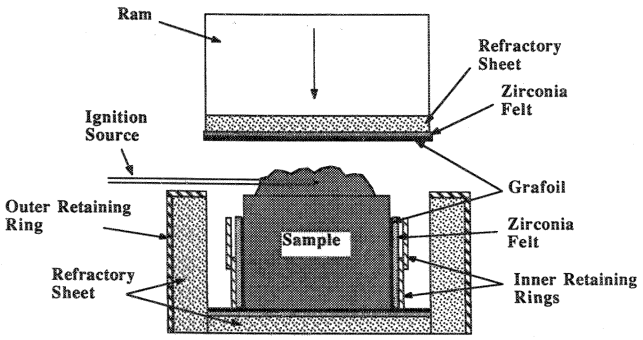

Fig. 1 — Schematic representation of specimen reaction and containment assembly.

retaining ring with a radial layer of alumina-zirconia refractory sheet (Zircar Products, Inc., Florida, NY), as shown schematically in Figure 1. Layers of ZrO_2 felt (Zircar Products, Inc., Florida, NY) and GRAFOIL* (Electronics Division, Union Carbide Corporation, Cleveland, OH) were placed around the compact to thermally insulate it. A 4-mm gap between the GRAFOIL and the powder compact was found to be sufficient for escape of the impurity gases during synthesis. Refractory sheet was also used as insulation in the axial direction. The refractory sheet affixed to the end of the forging ram, upon impact, wedged into the fixture, both consolidating the material and creating a fully closed, insulated system. A small amount of the loose Ti + B powder mixture was placed on top of the green compact, with an electric ignitor (Estes Industries, Penrose, CO) placed within the powder as an ignition source.

*GRAFOIL is a trademark of Union Carbide Corporation, Danbury, CT.

The reaction-consolidation fixture was placed within the lower die cavity of a modified Dynapak Model 400 metalworking machine capable of impact velocities of 5 to 15 m/s. Details of the Dynapak are given in Figure 2; it is described elsewhere.[8] Once securely located within the lower die cavity, the electric ignitor was remotely activated, igniting the loose starting powder, which, in turn, ignited the green powder compact. Depending on the composition, the reaction generally proceeded to completion within 3 to 5 seconds of ignition, and its progression could be verified by visual observation. Approximately 2 to 5 seconds after completion of the reaction, the forging hammer was activated and impacted the hot reaction product at velocities of 5 to 15 m/s. In this manner, dynamic consolidation of the ceramic was achieved while it remained at a temperature above its ductile to brittle transition (1600 °C to 1800 °C).[9] During compaction, a time-resolved history of the ram movement was recorded for determination of impact velocity. Following compaction, the specimen reaction-consolidation fixture was removed from the Dynapak lower die cavity and either inserted into an argon atmosphere furnace at a temperature of 1300 °C, or allowed to cool in air. Furnace samples were cooled over a period of 48 hours, while air cooling ensured much shorter times.

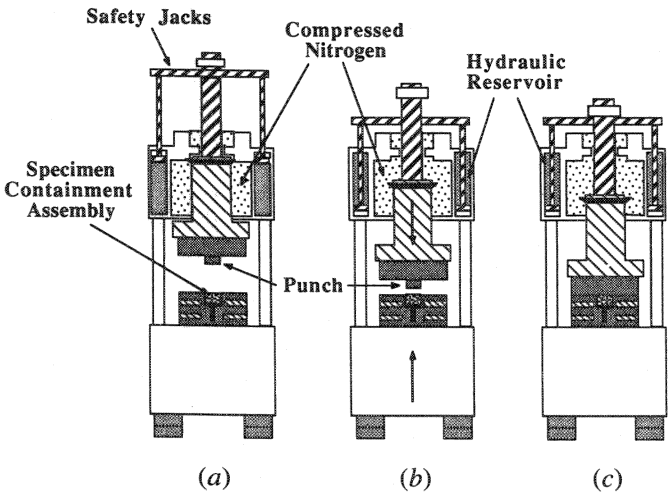

Fig. 2 — Sequence of events leading to dynamic compaction in Dynapak machine: (*a*) punch blocked by safety jacks, (*b*) machine in ready position after lowering of safety jacks, and (*c*) piston as it accelerates toward specimen containment assembly.

Significant lateral spreading of the sample during compaction was found to result in excessive cracking around the edges of the samples and hinder densification. Further experiments were performed where two separate telescoping mild steel rings 2.0- and 1.5-mm thick and 19.1-mm high, having diameters slightly larger than the green compact, were placed within the insulating ring to provide lateral confinement during the compaction step. Use of the telescoping retaining rings (shown in Figure 1) eliminated the air gap around the specimen; the exposed top surface of the compact was found to be sufficient to allow the reaction gases to escape. Other laterally confined experiments were performed in which the amount of presynthesized TiB_2 was decreased from 22 wt pct to 15 wt pct and in which 1.5 wt pct Ni (Aldrich Chemical Co., Milwaukee, WI) was added. The nickel purity was specified at 99.5 pct, and the particle size was 3 μm. The reaction and compaction procedures for these experiments were identical to those for the unconfined reactions.

Because of porosity, circumferential cracks, and material delaminations at the edges, densities were obtained from pieces cut from the central regions of the compacted samples. Densities were measured by a water immersion technique and normalized to the theoretical densities of TiB_2 (4.52 g/cm^3) and TiB_2 + 1.5 wt pct Ni (4.55 g/cm^3). The theoretical density of the nickel-containing samples was calculated by simple rule of mixtures.

Specimens for metallography, microhardness measurements, and electron microscopy were also obtained from the central regions of the samples. Hardness measurements were performed at room temperature using a Vickers indenter and a 300-g load. The values reported here are averages from at least 40 individual measurements with the standard deviation indicated. Polished and etched cross sections and fracture surfaces from the samples were examined by scanning electron microscopy (SEM) for general features, grain structure, and fracture modes using a Cambridge 360 unit. A piece of conventionally hot-pressed TiB_2 (Cercom Inc., Vista, CA) was obtained for property and structure comparisons. X-ray

microanalysis was performed on the compacted product to examine impurity and phase content.

Substructural differences in the TiB_2 as a function of fabrication technique were studied using transmission electron microscopy (TEM). Samples of the SHS and hot-pressed TiB_2 were sectioned for TEM examination using a low-speed diamond saw into wafers nominally 250-μm thick. Disks 3 mm in diameter were ultrasonically cut from the wafers. The disks were mechanically dimpled using 3-μm diamond paste to a center thickness of 25 μm. The disks were then ion thinned at approximately -150 °C using a 6 kV ion source at a grazing angle of 10 to 15 degs. Foils were observed at 200 kV using a JEOL 2000EX unit equipped with a double-tilt stage.

Room-temperature, low strain-rate (10^{-5} s^{-1}) compression tests were performed on the SHS/DC (dynamic compaction) and hot-pressed TiB_2 to determine the quasi-static strength and fracture modes. Details of the experimental setup are described elsewhere.[10] Room-temperature, high strain-rate (10^2 s^{-1}) compression tests were performed on the SHS/DC TiB_2 using a split Hopkinson pressure bar. Details of this equipment and experimental procedures are given elsewhere.[11] The specimens were rectangular and had dimensions of 4.1 × 4.1 × 8.1 mm; they were compressed along the long axis. For quasi-static testing, the specimens were placed between aligned tool steel plates hardened to 62 HRC with MoS_2 lubrication in a fixture developed at IFAM, Bremen, Germany. For the split Hopkinson pressure bar experiments, the specimens were placed between tungsten carbide disks attached to the ends of the incident and transmitter bars. These tungsten carbide disks were impedance matched to the maraging steel bars. The pulse front was tailored to provide a loading rate yielding a strain rate of 10^2 s^{-1}; this was accomplished by a pulse shaper (copper disk) placed between the striker bar and incident bar.[12] Resistive strain gages were used to measure the strain in the specimen throughout the test for both the quasi-static and dynamic testing.

III. RESULTS AND DISCUSSION

A. *Synthesis and Compaction*

The density and microhardness values for the TiB_2 disks produced by the SHS/DC process as a function of impact velocity and containment are listed in Table I. The densities for the laterally confined and unconfined specimens varied from 88 to 91 pct of the theoretical density of titanium diboride (4.52 g/cm^3). Sample densities for the laterally confined cemented (1.5 wt pct Ni) specimens varied from 94 to 96 pct of the calculated theoretical density (4.55 g/cm^3). Figure 3 shows the density *vs* impact velocity, or specific energy, for 8.5 cm × 1 cm TiB_2 and TiB_2-Ni disks. It is clear that a specific energy higher than 78 J/g is needed to densify the hot and porous TiB_2. The effect of nickel addition is very significant: an increase in density from 90 to 96 pct is obtained at a specific energy level of 74 J/g. Confinement also affects the final density; the additional heat extraction due to the telescoping steel rings leads to an increase of the strength of the reaction product at the moment of compaction, leading to a decrease in density, in comparison with unconfined specimens. X-ray microanalysis indicated complete material conversion to single-phase TiB_2 from the starting powders with no appreciable impurity content, as shown in Figure 4.

The top and bottom surfaces of the unconfined compacted samples generally did not exhibit major cracking. Figure 5 shows the top and bottom surfaces of SHS/DC TiB_2. One can see circumferential cracks (arrow A) in the periphery, while the center is crack-free. The refractory sheet (arrow B) can also be seen. For lower density samples, an increase of cracking in the bottom surface was evident, possibly indicating that the sample had cooled significantly before compaction. For all of the unconfined samples, the periphery exhibited circumferential cracks with material delaminations appearing throughout the edges. Expulsion of some of the reacting powders from the edges by hot impurity gases during synthesis may partially explain the fact that the edges of these

Table I. Microhardness of SHS/DC and Hot-Pressed TiB_2

Sample	Impact Velocity (m/s)	Lateral Confinement*	ρ/ρ_{th} (Pct Theoretical)	Microhardness (GPa) HV (300 g)
TiB_2				
1	10.2	N	87.5	20.9 ± 7.2
2	11.9	N	89.6	21.6 ± 6.9
3	12.5	N	91.0	23.8 ± 6.1
4	13.2	N	89.7	22.4 ± 4.9
5	13.5	N	90.4	21.4 ± 5.7
6	13.8	N	90.6	20.7 ± 7.4
7	13.8	Y	88.0	N/A
8	12.6	Y	84.4	N/A
TiB_2-Ni				
1	11.4	Y	94.3	N/A
2	12.6	Y	95.2	26.3 ± 2.6
3	13.8	Y	96.1	27.6 ± 2.5
Hot pressed				
HP	N/A	N/A	99+	27.8 ± 2.1

*N = no; Y = yes; and N/A = not analyzed

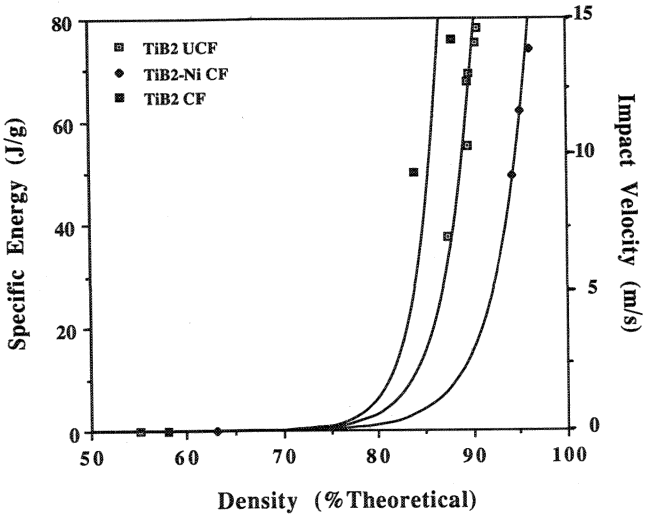

Fig. 3—Density *vs* impact velocity (or specific energy) for three experimental conditions: titanium diboride in laterally confined (CF) and unconfined (UCF) assembly and laterally confined (CF) titanium diboride + 1.5 wt pct Ni.

samples are not as crack-free as the central regions. Also, significant lateral spreading associated with the application of the compacting force resulted in less material at the edges and could have caused additional cracking. In the case of the laterally confined samples, the problem of edge cracking was eliminated. However, in most cases, the retaining rings were heavily deformed, and the tendency for surface cracking increased. This is not surprising, since the steel retaining rings tend to act as a heat sink at the high reaction temperatures, increasing

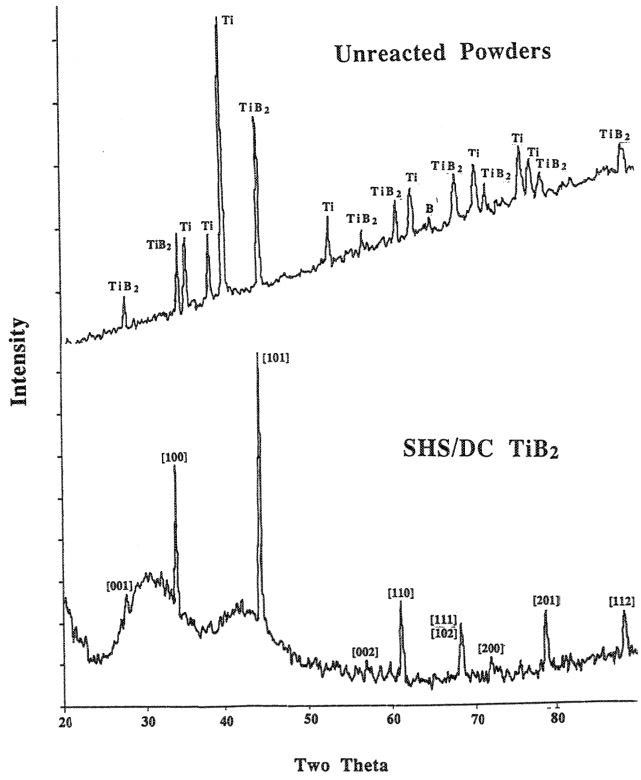

Fig. 4—X-ray diffractometer traces of unreacted and reacted + compacted material, showing full conversion to single-phase TiB_2.

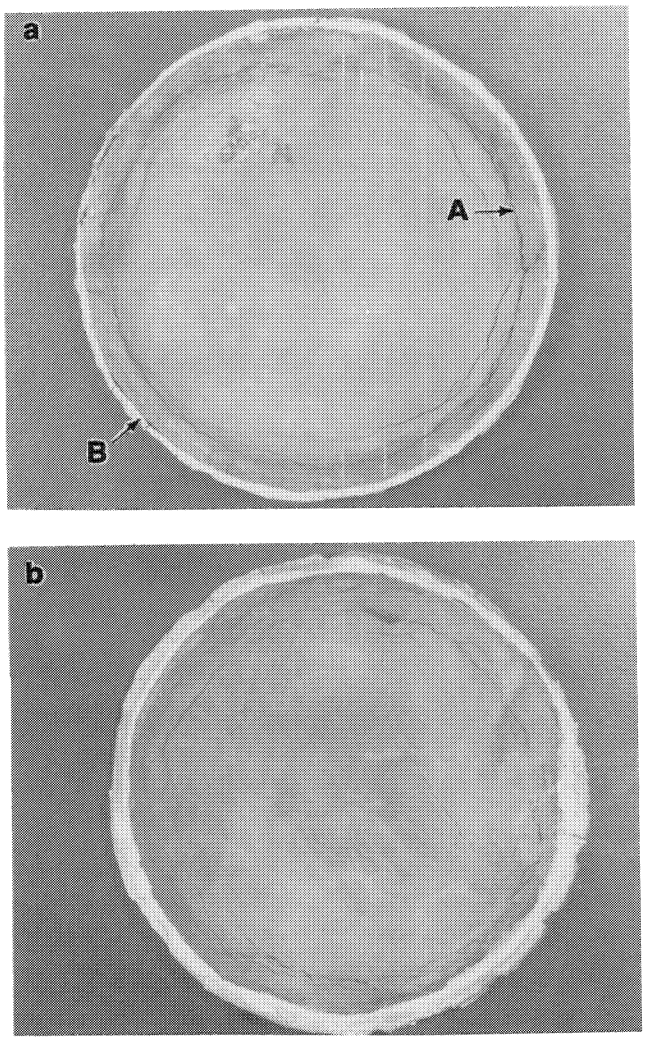

Fig. 5—Titanium diboride disk with diameter of 8.5 cm and thickness of 1.0 cm: (*a*) top and (*b*) bottom. Radical cracks shown by arrow A; residual refractory sheet shown by arrow B.

the heat flow away from the reacted sample, reducing material plasticity, and producing surface cracks; a detailed analysis is being conducted by Meyer *et al.*[13]

B. *Mechanical Properties*

Table I shows the microhardness of the SHS/DC and hot-pressed TiB_2. They vary from 20.7 to 27.6 GPa and correlate well with the density. The highest hardness, 27.6 GPa, was obtained for a specimen which exhibited a density of 96.1 pct. This hardness is essentially identical to the hot-pressed TiB_2. The variation in hardness was a direct result of the ability to place the indenter in a void-free region of the sample without the collapse of adjacent grains.

Quasi-static (10^5 s^{-1}) and dynamic (10^2 s^{-1}) compressive test results are shown in Table II. There does not seem to be a significant effect of strain rate on compressive strength, although the dynamic test results are incomplete. The compressive strength of SHS/DC TiB_2 is approximately 1.7 to 2.0 GPa. This is significantly lower than the compressive strength of hot-pressed TiB_2.

Table II. Quasi-Static (10^{-5} s^{-1}) and Dynamic (10^{2} s^{-1}) Compressive Strength of SHS/DC and Hot-Pressed TiB_2

Sample	ρ/ρ_{th} (Pct Theoretical)	Quasistatic		Dynamic	
		σ (GPa)	E (GPa)	σ (GPa)	E (GPa)
1	87.5	1.57	410	1.94	440
5	89.7	1.78	441	N/A*	N/A
9	90.6	1.87	435	1.88	428
10	90.4	N/A	N/A	2.03	454
HP	99+	4.21	600	N/A	N/A

*N/A = not analyzed

The differences in elastic moduli are also significant: approximately 420 GPa for SHS/DC TiB_2 and approximately 600 GPa for hot-pressed TiB_2. These differences contrast with the hardness values that are approximately equal. One can speculate that the differences are due to microcracking, which would not significantly affect microhardness but which profoundly affects both the compressive strength and elastic modulus.

There are two principal sources for the decrease of the Young's modulus, porosity and microcracking. The change in Young's modulus with porosity has been analytically expressed by Wachtman[14] and MacKenzie:[15]

$$E = E_0 (1 - f_1 p + f_2 p^2)$$

where p is the porosity and f_1 and f_2 are constants. For the porosity of the SHS/DC TiB_2, one finds a decrease in E from 600 to 480 GPa. A modulus of 600 GPa is consistent with the highest values reported by Castaing and Costa.[16] However, Young's modulus of the SHS/DC TiB_2 was 30 pct lower (440 GPa) than the conventionally processed TiB_2 (600 GPa). If one considers microcracking, further decreases in E are obtained. Microcracking has been treated by O'Connell and Budiansky[17] and Salganik[18] in tension and Nemat-Nasser and Horii[19,20,21] in compression. The expression developed by Salganik[18] is

$$\frac{E}{E_0} = \left[1 + \frac{16(10 - 3\nu_0)(1 - \nu_0^2)}{45(2 - \nu_0)} Na^3 \right]^{-1}$$

where E is Young's modulus of the cracked ceramic, ν_0 and E_0 are Poisson's ratio and Young's modulus of the uncracked material, respectively, a is the radius of a mean crack, and N is the number of cracks per unit volume. The microcrack size and density can be estimated from Figure 6. Assuming a Poisson's ratio of 0.11,[16] a mean crack radius of approximately 4 μm, and one microcrack per grain (average diameter equal to 15 μm), the microcrack population within the SHS/DC TiB_2 has the effect of lowering the Young's modulus from 480 GPa to approximately 450 GPa. Assuming that the effects of voids and cracks on the Young's modulus are additive, the low values obtained experimentally can be explained. Therefore, one must not overlook the effect of porosity and microcracking on Young's modulus.

C. *Microstructure*

Scanning electron microscopy of the SHS/DC TiB_2 revealed a microstructure consisting of randomly oriented faceted grains on the order of 10 to 20 μm, partially sintered grains, and intergranular and intragranular voids. Figure 6(a) shows the polished and etched surface of SHS/DC TiB_2 where the light gray areas are void-free TiB_2 and the black areas are intergranular voids. The interior of the intergranular voids appear to be uncompacted TiB_2. The interior void structure appears to be remnant porosity from the green compact, indicating that either the energy was not sufficient to totally collapse voids or that confinement was not adequate. Evidence of microcracking (arrow A) is seen within most of the grains. Figure 6(b) shows the microstructure of SHS/DC TiB_2 with 1.5 wt pct Ni. The polished and etched surface shows excellent bonding between grains with nickel residing at the grain boundaries (arrow A). The grain morphology is distinctly different from that of the pure SHS/DC TiB_2 in that the grains appear equiaxed; no microcracks can be seen. This improved structure is due to the increased reaction temperature as a result of the decrease in presynthesized TiB_2 (from 22.5 to 15 wt pct); adiabatic combustion temperature calculations indicate an increase of approximately 250 K in the reaction temperature. As a result, the combination of increased reaction temperature and added Ni overshadowed any detrimental heat loss effects from the steel retaining rings. The structure of the hot-pressed TiB_2 is significantly different from that of either the SHS/DC TiB_2 or TiB_2-Ni, as shown in Figure 6(c); its microstructure consists of equiaxed grains on the order of 5 to 10 μm, with a sintering aid present at the grain boundary triple points and along some grain boundaries (arrow A). This material exhibited a large number of voids within the grains and cracks along some grain boundaries (arrows B and C, respectively).

Transmission electron microscopy of the SHS/DC TiB_2 revealed some intragranular (grain interior) porosity, in addition to the intergranular porosity seen by SEM (Figure 6(a)). The intragranular pores tended to be faceted, as shown in Figure 7. Some inclusions are also noticeable. Another feature of the SHS/DC TiB_2 is the substantial density of dislocations seen in many grains. Figure 8 shows an area within the SHS/DC TiB_2 of varying grain size in which the larger grains tend to be relatively free of dislocations and the smaller surrounding grains exhibited high dislocation densities. It was not possible to identify the presynthesized TiB_2 and to differentiate it from the reaction-synthesized material.

One possible explanation as to the origin of the high dislocation densities arises from the fact that 22 wt pct pre-synthesized TiB_2 was added to the reacting mixture as a diluent. Because the pre-synthesized TiB_2 powder had the effect of reducing the combustion temperature,

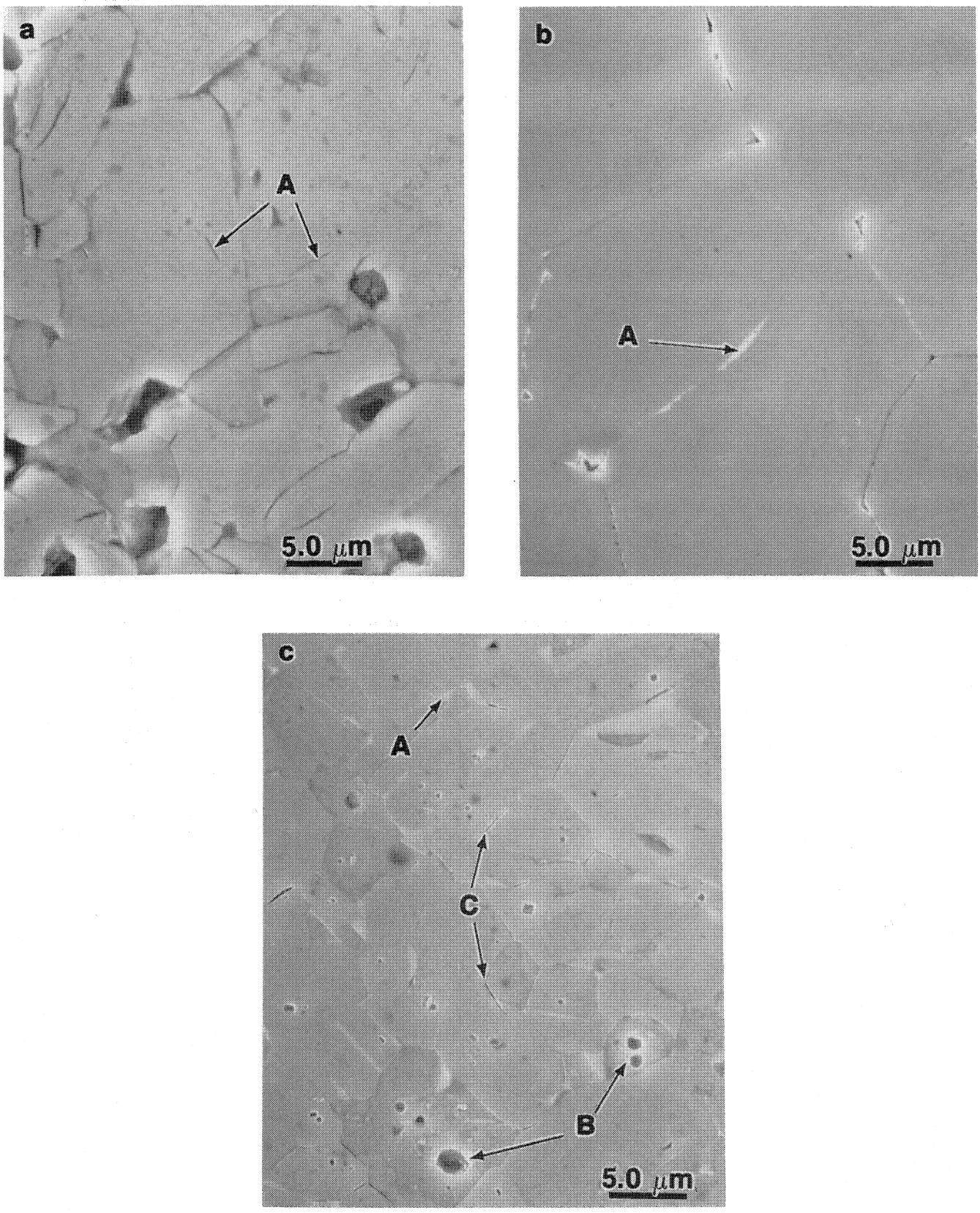

Fig. 6—Polished and etched surfaces of (*a*) SHS/DC TiB_2, evidence of microcracking shown by arrow A; (*b*) SHS/DC TiB_2 + 1.5 wt pct Ni, nickel residing at the grain boundaries shown by arrow A; and (c) hot-pressed TiB_2, presence of sintering aid (arrow A), intragranular voids (arrow B), and grain boundary cracks (arrow C) (viewed by SEM).

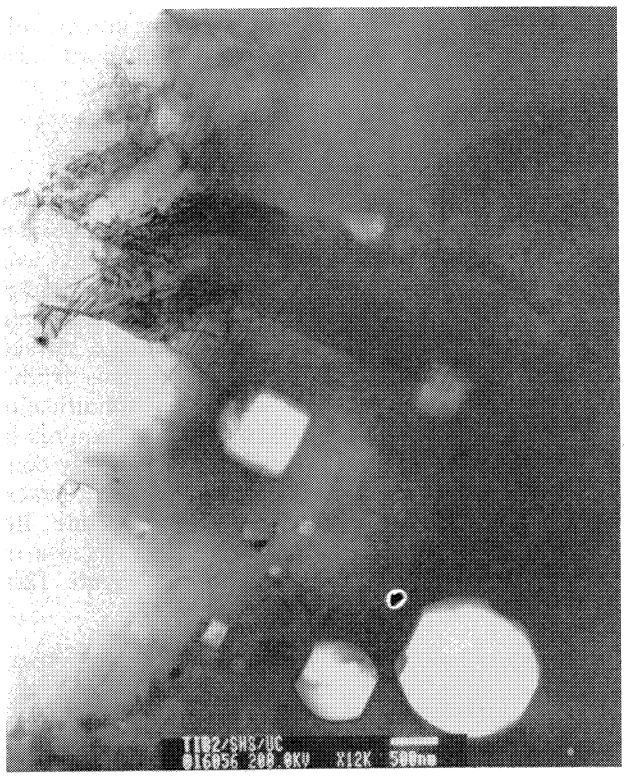

Fig. 7—Faceted intragranular voids in SHS/DC TiB_2 as viewed by TEM.

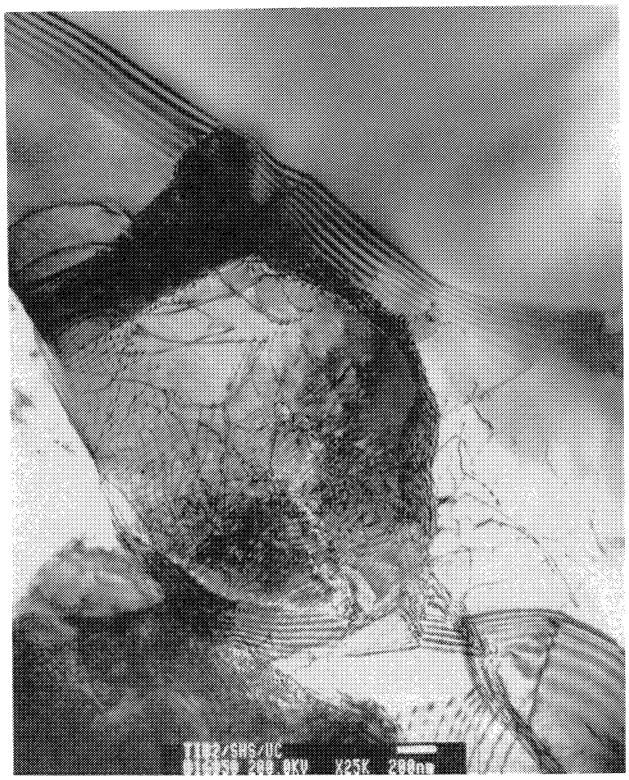

Fig. 8—Dislocations in SHS/DC TiB_2 as viewed by TEM.

Fig. 9—Grain structure of hot-pressed TiB_2 as viewed by TEM.

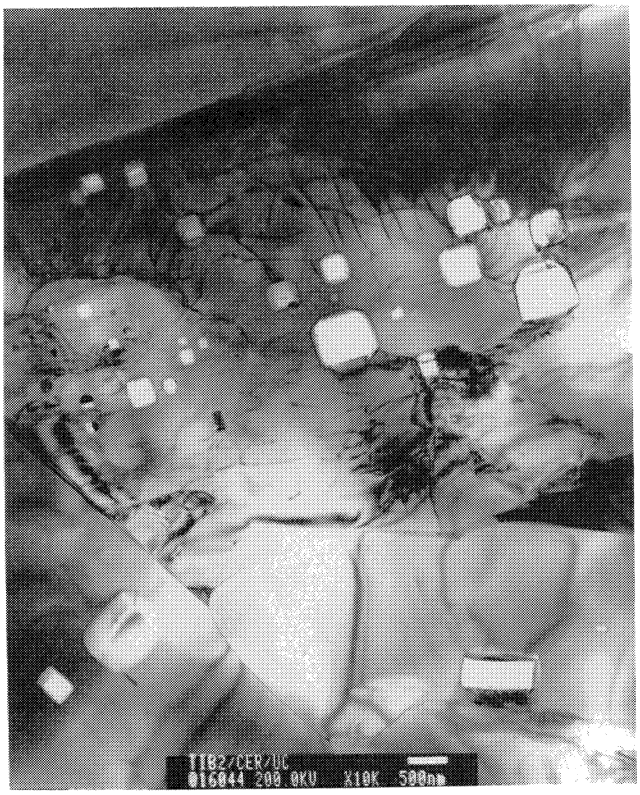

Fig. 10—Intragranular faceted voids in hot-pressed TiB_2 as viewed by TEM.

the possibility exists that the diluent was only partially melted or not melted at all at the time of impact. Therefore, if the diluent was not sufficiently plastic, it would tend to take the brunt of the deformation stresses upon impact, forming dislocations in response to the applied load. The differences in grain size and dislocation density can be due to the reason above or due to substructure recovery processes (recovery and/or recrystallization) during or after plastic deformation.

The hot-pressed TiB_2 was found to be a mixture of mostly equiaxed grains with some that were rather rectangular in shape (Figure 9). A limited number of dislocations were evident within the grains, primarily pinned at inclusions or intragranular voids. Also identified was a second phase residing at the grain boundary triple points and along some grain boundaries; this is the sintering aid. The presence of a sintering aid within the hot-pressed TiB_2 helps to increase its density and compensates for the porosity. Figure 10 shows that a typical cross section of the hot-pressed material contains some intragranular voids. There are also some regions which contained square or hexagonal inclusions.

D. *Fracture Characteristics*

Fractographs from SHS/DC TiB_2 samples tested at low strain rate revealed failure *via* transgranular mode. The fracture surface, as shown in Figure 11(a), reveals cleaved grains, intragranular (arrow A) and intergranular porosity (arrow B). Figure 11(b) shows an area of partially compacted SHS TiB_2 exposed by the fracture surface. The surfaces within these uncompacted regions exhibit, in some cases, ledges that are due to the solidification process and, in other cases, are rounded, as required by the minimization of surface energy. The partially compacted regions of the samples, as well as microcracks within the grains, are nucleation sites for fracture. Impact fracture surfaces of the SHS/DC TiB_2-Ni also revealed failure *via* transgranular fracture. Figure 12(a)

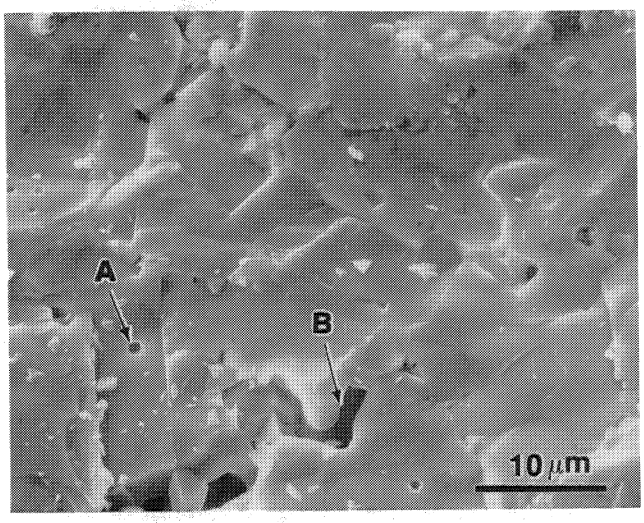

(*a*)

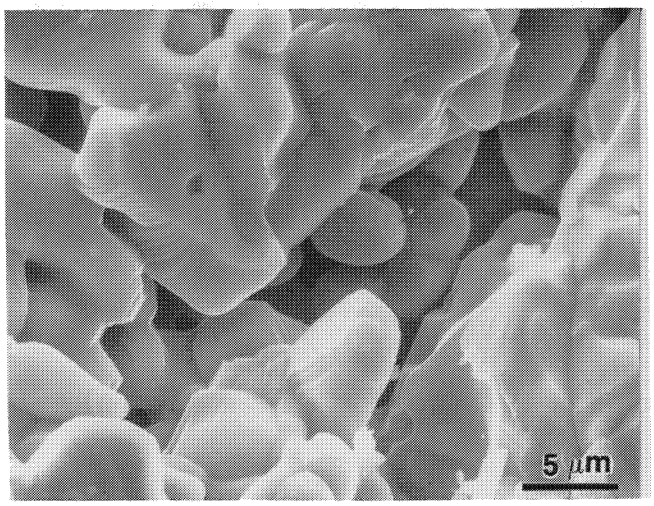

(*b*)

Fig. 11 — Scanning electron micrographs of SHS/DC TiB_2 fracture surface produced in quasi-static compression test (10^{-5} s^{-1}): (*a*) transgranular fracture showing small intragranular (arrow A) and larger intergranular (arrow B) voids and (*b*) large intergranular void.

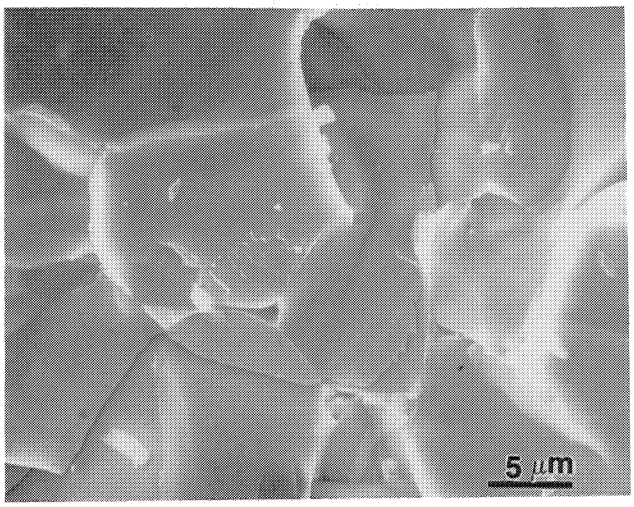

(*a*)

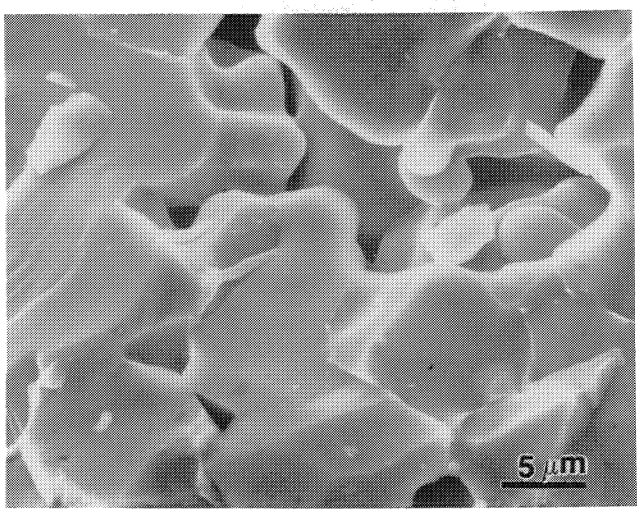

(*b*)

Fig. 12 — Scanning electron micrographs of SHS/DC TiB_2 + 1.5 wt pct Ni fracture surface produced by impact loading: (*a*) fracture morphology and (*b*) intergranular voids.

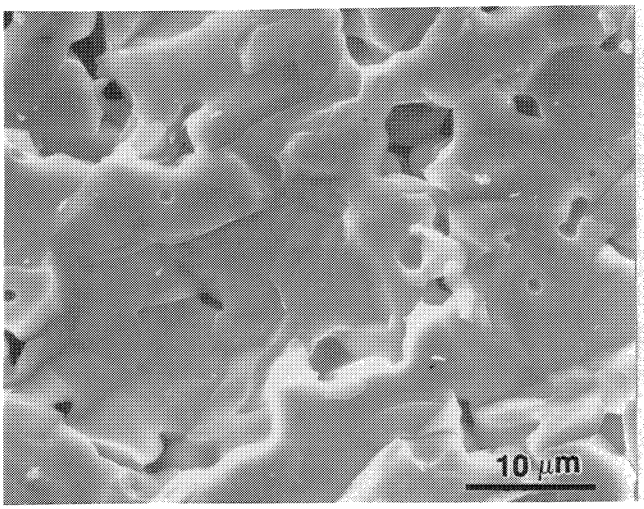

Fig. 13—Scanning electron micrograph of SHS/DC TiB_2 fracture surface produced in high strain-rate compression test (10^2 s^{-1}) showing transgranular fracture.

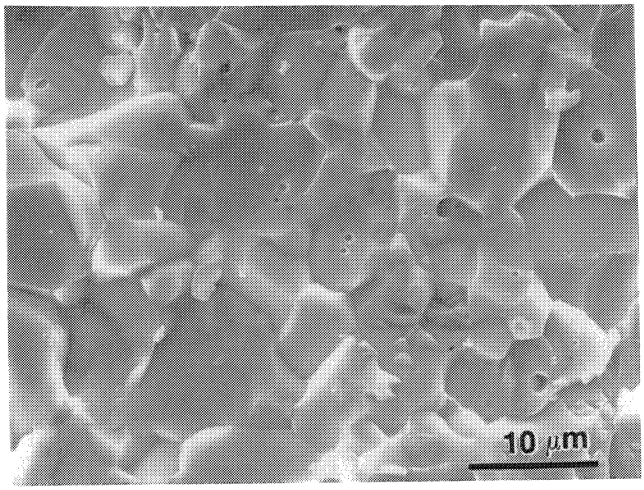

(*a*)

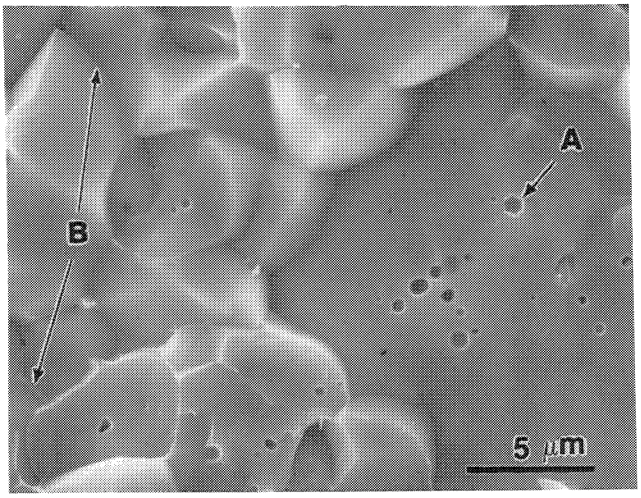

(*b*)

Fig. 14—Scanning electron micrographs of hot-pressed TiB_2 fracture surface produced by impact loading: (*a*) mixed transgranular-intergranular fracture mode and (*b*) population of intragranular (faceted) voids (shown by arrow A) and intergranular phase (shown by arrow B).

shows the fracture surface of an SHS/DC TiB_2-Ni, with some evidence of uncompacted regions within the sample, as shown in Figure 12(b). This condition exhibited less porosity than the SHS/DC TiB_2. Nevertheless, partially compacted regions (intergranular pores) could be identified. One such region is shown in Figure 12(b). The SHS/DC TiB_2 high strain-rate fracture surfaces (Figure 13), produced by the split Hopkinson pressure bar, were essentially identical to the low strain-rate surfaces; thus, the fracture mode remains unchanged at high strain rates.

Hot-pressed TiB_2 fracture surfaces differed from the SHS material in that both a transgranular and intergranular fracture component were evident. Figure 14(a) shows the general features of the fracture surface of a hot-pressed TiB_2. Figure 14(b) shows faceted and irregularly shaped intragranular pores within the cleaved grain of the hot-pressed TiB_2. One can also see the sintering phase at the grain boundaries, marked by an arrow.

IV. CONCLUSIONS

It has been demonstrated that titanium diboride produced by reaction synthesis can be consolidated in a high-velocity forging machine. The compacts exhibit circumferential cracks but have extensive crack-free regions. Compressive tests carried out at quasi-static and dynamic strain rates showed that the strength is approximately 1.8 GPa.

Characterization of the SHS/DC TiB_2 by TEM revealed that the plastic deformation during consolidation generated profuse dislocations. There is evidence that some regions undergo recrystallization.

Micro- and macrocracking during and after consolidation are major problems, and it is thought that thermal gradients play an important role in their formation.

ACKNOWLEDGMENTS

This research was supported by the Army Research Office under Contract No. ARO-DAAL-03-88-K-0194. The help provided by Mr. Klaus Bluegell throughout this investigation, by modifying and operating the Dynapak unit, was invaluable; his dedication is greatly appreciated. Mr. J. LaSalvia provided valuable advice throughout this investigation. Mr. Jon Isaacs was instrumental in the conduction of the dynamic compaction tests in the split Hopkinson pressure bar and in the measurement of the Dynapak piston velocity; we appreciate his dedicated help. The help of Mr. Subhash Ghatuparthi in dynamic testing is also acknowledged. The use of the facilities of the Center of Excellence for Advanced Materials is greatly appreciated. The hot-pressed TiB_2 was obtained from Cercom Inc., Vista, CA, and we thank Mr. Richard Polyka for his help.

REFERENCES

1. A.G. Merzhanov: in *Combustion and Plasma Synthesis of High-Temperature Materials*, Z.A. Munir and J.B. Holt, eds., VCH Publishers, New York, NY, 1990, p. 1.

2. Z.A. Munir and U. Anselmi-Tamburini: *Mater. Sci. Rep.*, 1989, vol. 3, pp. 227-365.
3. Z.A. Munir: *Am. Ceram. Soc. Bull.*, 1988, vol. 67, pp. 342-49.
4. H.C. Yi and J.J. Moore: *J. Mater. Sci.*, 1990, vol. 25, pp. 1159-68.
5. A. Niiler, L.J. Kecskes, T. Kottke, P.H. Netherwood, Jr., and R.F. Benck: Technical Report BRL-TR-2951, Ballistic Research Laboratory, Aberdeen Proving Ground, MD, Dec. 1988.
6. J.B. Holt and Z.A. Munir: *J. Mater. Sci.*, 1986, vol. 21, pp. 251-59.
7. J.C. LaSalvia, L.W. Meyer, D.A. Hoke, A. Niiler, and M.A. Meyers: in *Shock Waves and High-Strain-Rate Phenomena in Materials*, M.A. Meyers, L.E. Murr, and K.P. Staudhammer, eds., Marcel Dekker, New York, NY, 1992, p. 261.
8. J.C. LaSalvia: M.S. Thesis, University of California–San Diego, La Jolla, CA, 1990.
9. J.R. Ramberg and W.S. Williams: *J. Mater. Sci.*, 1987, vol. 22, pp. 1815-26.
10. E. Staskewitsch: *Fortschritts-Berichte VDI-Zeitschrift*, Verlag, Dusseldorf, Federal Republic of Germany, 1981, vol. 56, p. 5.
11. P.S. Follansbee: *Metals Handbook*, 9th ed., ASM, Metals Park, OH, 1985, vol. 8, p. 198.
12. W.P. Rogers and S. Nemat-Nasser: *J. Am. Ceram. Soc.*, 1990, vol. 73 (1), pp. 136-39.
13. L.W. Meyer, J.C. LaSalvia, and M.A. Meyers: IFAM, Bremen, Federal Republic of Germany, University of California–San Diego, unpublished research, 1991.
14. J.B. Wachtman: in *Mechanical and Thermal Properties of Ceramics*, J.B. Wachtman, ed., NBS Special Publication 303, NBS, Washington, DC, 1963, p. 139.
15. J.K. MacKenzie: *Proc. Phys. Soc.*; 1950, vol. B63, p. 2.
16. J. Castaing and P. Costa: in *Boron and Refractory Borides*, V.I. Matkovich, ed., Springer-Verlag, Berlin, 1977, p. 390.
17. J. O'Connell and B. Budiansky: *J. Geol. Res.*, 1974, vol. 19, p. 5412.
18. R.L. Salganik: *Izr. Akad. Nauk., SSR, Mekh. Tverd. Tela*, 1973, vol. 8, p. 149.
19. S. Nemat-Nasser and M. Horii: in *Micromechanics and Inhomogeneity*, H. Weng, ed., Springer-Verlag, New York, NY, 1990, p. 297.
20. M. Horii and S. Nemat-Nasser: *J. Geophys. Res.*, 1985, vol. 90, p. 3105.
21. M. Horii and S. Nemat-Nasser: *Phil. Trans. R. Soc.*, 1986, vol. 319, p. 337.